Journal of Power Sources 216 (2012) 297–303

Contents lists available at SciVerse ScienceDirect

Journal of Power Sources

journal homepage: www.elsevier.com/locate/jpowsour

Glucose microfluidic fuel cell based on silver bimetallic selective catalysts for on-chip applications

F.M. Cuevas-Muñiz [a], M. Guerra-Balcázar [a], J.P. Esquivel [c], N. Sabaté [c], L.G. Arriaga [b,*], J. Ledesma-García [a]

[a] Division de Investigación y Posgrado, Facultad de Ingeniería, Universidad Autónoma de Querétaro, Cerro de las campanas s/n, 76010 Santiago de Querétaro, Mexico
[b] Centro de Investigación y Desarrollo Tecnológico en Electroquímica, Parque Tecnológico Querétaro Sanfandila, Pedro Escobedo 76703, Querétaro, Mexico
[c] Instituto de Microelectronica de Barcelona, IMB-CNM (CSIC) Campus UAB, 08193 Bellaterra, Barcelona, Spain

HIGHLIGHTS

- Glucose microfuel cell with outstanding performance at zero flow condition is showed.
- Bimetallic materials based on Ag exhibit tolerance to byproducts and crossover effect.
- Microfluidic fuel cell was evaluated with a simulated body fluid solution at zero flow.
- This fuel cell can be used as a portable power source in Lab-on-a-Chip applications.

ARTICLE INFO

Article history:
Received 18 April 2012
Received in revised form
22 May 2012
Accepted 23 May 2012
Available online 1 June 2012

Keywords:
PtAg nanoparticles
AuAg nanoparticles
Simulated body fluid

ABSTRACT

A glucose microfluidic fuel cell with outstanding performance at zero flow condition is presented. Polarization tests showed that bimetallic materials based in silver (AuAg/C as anode, PtAg/C as cathode) exhibit tolerance to byproducts and crossover effect. This allowed achieving one of the highest power densities reported for glucose fuel cells, up to a value of 630 $\mu W\ cm^{-2}$ using two separated laminar flows of reactants. Furthermore, the tolerance to crossover effect caused by the selectivity of PtAg/C to oxygen reduction reaction in presence of glucose permitted using a single flow containing a mixture of glucose/oxygen, yielding a performance as high as 270 $\mu W\ cm^{-2}$. Microfluidic fuel cell was further evaluated with a simulated body fluid solution that contained salts commonly present in the human blood plasma, reaching a power of 240 $\mu W\ cm^{-2}$ at zero flow. These results envisage the incorporation of this fuel cell as a portable power source in Lab-on-a-Chip devices without the need of external pumps.

1. Introduction

In recent years, Lab-on-chip (LOC) has gained attention because of its many advantages in chemical analysis. LOC devices integrate different stages of chemical analysis within reduced dimensions. LOC devices have numerous applications such as biological and chemical analysis, point-of-care testing, clinical and forensic analysis, molecular diagnostics and medical diagnostics [1]. Nevertheless, LOCs are still not completely autonomous because they lack of integrated power sources, which provide enough energy to the devices. Currently, microbatteries and RF devices represent the most common solutions. However, RF devices are limited to the distance from the power source and batteries must be recharged or replaced. In this sense, microfuel cells are an attractive alternative because they can operate as long as fuel is supplied [2]. However, the miniaturization of fuel cells is a complex process, because of components as the membrane lost its performance when it is reduced in width. Microfluidics avoid the mixture of fuel and oxidant flows, because of lack of turbulence of the fluids [3–6]. In microfluidic fuel cells, one stream with fuel and another with oxygen are introduced in a microchannel that can incorporate the electrodes on its walls. This configuration allows the manufacturing of smaller devices.

Different power sources have been used for fuel cells, including formic acid [6], glycerol [7], ethylene glycol [8] and glucose [9]. Glucose presents advantages such as low toxicity, biocompatibility, and low cost. Also glucose is found in all the living organisms as an energy source, making possible to incorporate glucose-based devices for in vivo applications without the need for an external fuel feeding. The use of glucose, however, has still many issues to resolve such as slow kinetics, poor efficiency or material inactivation [10]. Fuel cells have been proved to operate in physiological media for in vivo applications, but have been mostly used in simple

* Corresponding author. Tel.: +52 4422116069; fax: +52 4422116000.
E-mail address: larriaga@cideteq.mx (L.G. Arriaga).

0378-7753/$ – see front matter © 2012 Elsevier B.V. All rights reserved.
doi:10.1016/j.jpowsour.2012.05.101

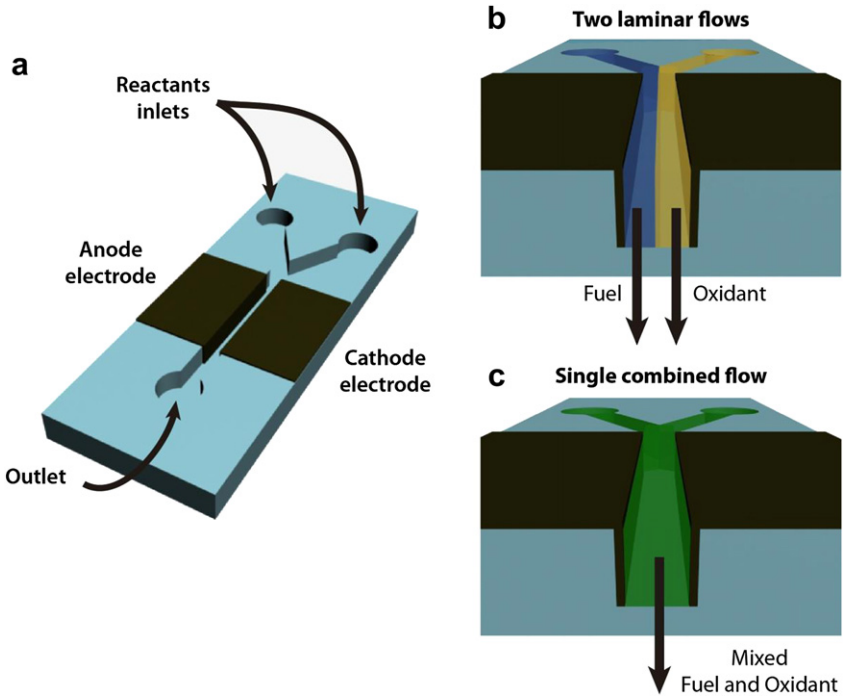

Fig. 1. Microfluidic component used in this study, a) Y-shape microchannel and electrodes, b) operation with two separated laminar flows and c) operation with a single combined flow.

matrices (support electrolyte and/or buffer) [6,11–15]. Some works have been performed in phosphate buffer solution (PBS) [16–18]. There are few reports in vivo conditions [18] of nearly in vivo [19].

In order to obtain a better performance of glucose fuel cells, different catalytic materials have been evaluated. Inorganic and biological catalysts have been proven. Enzymes have high selectivity and high kinetics, but are sensitive to media conditions and present stability problems [20–22]. On the other hand, noble metals like gold and platinum can operate in a wide range of conditions, but present poisoning troubles and low selectivity [23–26]. Bimetallic combinations like silver with gold [27,28] or platinum [29] have promising results for reducing poisoning and increase the selectivity, while reducing the cost of the materials involved in the cells construction.

In a previous article we reported the performance of bimetallic nanoparticles AuAg/C for the glucose oxidation reaction (GOR) in alkaline media. AuAg/C in contrast with Au/C exhibits a minor activity, but a good stability after 4 h of use [30]. On the other hand, we tested PtAg/C for oxygen reduction reaction (ORR). PtAg/C exhibited tolerance to high concentrations of glucose 0.1 M, meanwhile Pt/C was only able to work in glucose 0.01 M [31].

The objective of this work is the evaluation of a microfluidic fuel cell composed by selective catalysts based in silver. The catalysts allow the utilization of a single flow combining glucose as fuel and oxygen as oxidant in alkaline medium. The performance of the fuel cell was first tested using separated flows of oxidant and glucose at different concentrations. Then, the selectivity of the electrocatalysts was evaluated injecting a single flow with a mixture of both reactants. Finally, the system was tested using of a complex matrix (containing salts present in the extracellular fluid) as a first step toward the use of this fuel cell in biological applications. This solution was called SBF (simulated body fluid) and was based in the work of Kokubo, with slight modifications to adapt to the current experimental conditions [32]. This SBF was introduced to the fuel cell at different flow rates, demonstrating a correct operation even at zero flow conditions.

2. Experimental

2.1. Synthesis of bimetallic catalyst

The synthesis of bimetallic catalyst was carried out according to previous works using chemical reduction of metallic salts [30,31,33]. The initial solution were prepared with atomic ratio Au:Ag 80:20 and Pt:Ag 80:20. In this process the metallic salts, Chloroauric acid (JT Baker), silver nitrate (JT Baker), ammonium tetrachloroplatinate (Sigma–Aldrich), according the case, were placed in aqueous solution and mixed with tetraoctylammonium bromide (JT Baker) in toluene. After mixing 30 min, dodecanothiol (Sigma–Aldrich) was added and the mix was to cool at 2 °C. $NaBH_4$ (JT Baker) was added and leave for two and half hours. The materials obtained were supported in Vulcan XC-72 35 (Cabot) to 30% w/w by impregnation, and calcinated in a furnace at 350° by 3 h. Pt/C 30% was purchased from Etek.

2.2. Physicochemical characterization

The physicochemical characterization was performed by transmission electronic microscopy (TEM) using a JEOL 40 JEM2200Fs + Cs STEM. Scanning electron microscopy (SEM), X-ray diffraction (XRD) and electrochemical characterization was previously reported [30,31]. Bimetallic materials formation is evidenced from these techniques.

Table 1
Electrode materials and loading for the three microfluidic fuel cell configurations.

	Anode	Loading/mg cm^{-2}	Cathode	Loading/mg cm^{-2}
MFC1	Au	1.2	Pt	1.1
MFC2	Au	1.4	PtAg	1.3
MFC3	AuAg	1.4	PtAg	1.1

Table 2
Ionic concentrations in SBF before the addition of KOH.

Ionic species	Concentration/mM
Na^+	142.0
K^+	5.0
Mg^{2+}	1.5
Ca^{2+}	2.5
Cl^-	153.0
HCO_3^-	4.2
HPO^-	1.0
SO_4^{2-}	0.5

2.3. Microfluidic fuel cell setup

Microfluidic fuel cell setup used in this work has been described previously [5]. The device is composed of PMMA component in which a Y-shape microchannel has been defined by hot embossing at 140 °C and pressed to 24,000 lbs in^{-2}. The dimensions are 2 mm width, 1 mm high and 45 mm long. Anode and cathode current collectors were fabricated using XC72-Vulcan. Anode and cathode electrocatalysts have been incorporated on the microchannel walls using spray coating technique. Fig. 1 shows a schematic illustration of the device and the two operation modes used. Three microfluidic fuel cells were constructed, in which the catalyst materials for anode and cathode were varied as shown in Table 1.

2.4. Characterization with two laminar flows

Two solutions of D (+) glucose (Aldrich) at concentrations of 10 mM and 100 mM in 0.3 M KOH (J.T. Baker) were used as fuel, feeding the anode at a flow rate of 100 μL min^{-1} using a Single-Syringe Infusion Pump (Cole-Palmer 78-0100C).

Oxygen was passed through a saturation tower to be dissolved 60 (4.3 U.A.P Praxair) in 0.3 M KOH. This oxidant solution was fed to the cathode at 500 μL min^{-1} with a peristaltic pump (Cole-Palmer 7553-70). Polarization curves were recorded in a BioLogic VSP at 20 mV s^{-1}.

2.5. Characterization with a single combined flow

The microfluidic fuel cell performance was also evaluated introducing a single flow to the microchannel. The flow was composed by an oxygen saturated glucose solution (10 and 100 mM) in KOH 0.3 M. The solution was injected with a 60 mL syringe at 400 μL min^{-1} using a Single-Syringe Infusion Pump. Polarization curves were recorded in a BioLogic VSP at 20 mV s^{-1}.

2.6. Simulated body fluid (SBF) evaluation

A simulated body fluid (SBF) was prepared adding several salts, NaCl, KCl, $NaHCO_3$, K_2HPO_4, Na_2SO_4, $MgCl_2$, $CaCl_2$ and HCl (Table 2 shows the ionic concentration of each salt used). KOH was added to SBF to obtain 0.3 M in KOH and filtrated to avoid aggregates before adding glucose (1.8 g L^{-1}). The solution was oxygenated for 20 min and injected into the cell at 400 μL min^{-1}.

The microfluidic fuel cell performance was evaluated introducing the SBF solution at different volumetric flow rates, ranging from 500 to 0 μL min^{-1}.

Finally, an evaluation of the fuel cell stability at zero fluid flow was carried out. This evaluation was composed of five cycles of three steps each. In the first step, the cell was filled for 2 min with SBF at 200 μL min^{-1}. In the second step consisted of a waiting time

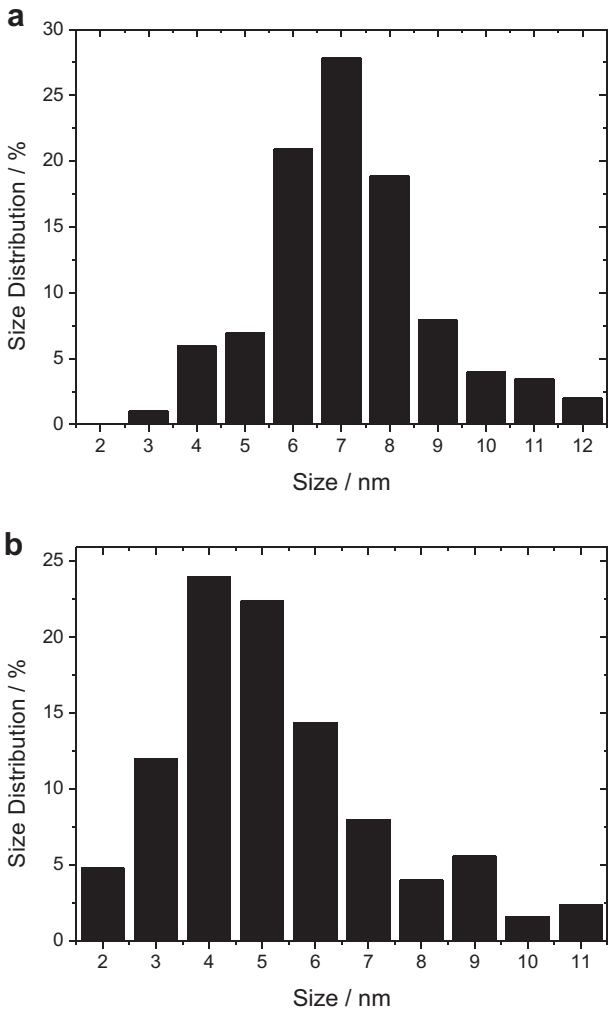

Fig. 3. Size distribution histograms for a) AuAg/C and b) PtAg/C.

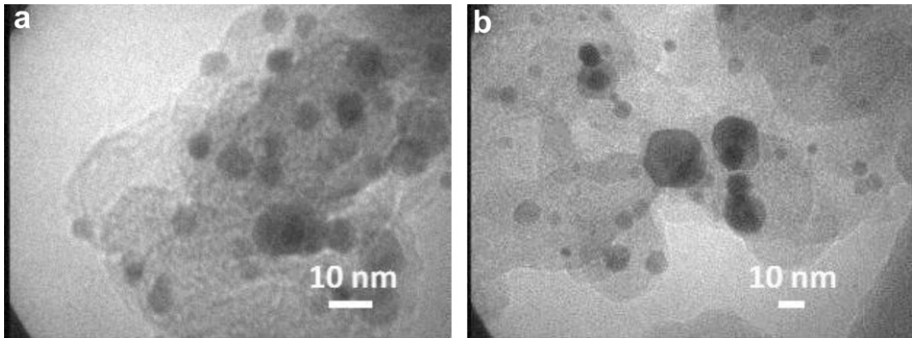

Fig. 2. Transmission electronic micrographies for a) AuAg/C and b) PtAg/C.

for 8 min with zero flow rate. In the third step was a chronoamperometry measurement at 320 mV for 10 min. Current and voltage during the whole cycling experiment were recorded.

3. Results and discussion

3.1. Physicochemical characterization

Transmission electronic micrographs are presented in Fig. 2. EDS analysis of the catalyst revealed that the atomic ratio in AuAg/C is 73.5% of Au and 26.5% of Ag. In the case of PtAg/C is 81% of Pt and 19% of Ag. These compositions are according with the concentration of the initial solution in the preparation. The nanoparticles size according with the TEM figures is 7 nm for AuAg/C and 4 nm for PtAg/C, the distribution is shown in Fig. 3.

3.2. Microfluidic fuel cell performance with two laminar flows

Fig. 4 shows the performance of the three different microfluidic cells (MFC1, MFC2 and MFC3) using 10 mM glucose + 0.3 M KOH (G10). MFC1 shows the best performance in comparison with MFC2 and MFC3, reaching a maximum power density of 450 W cm^{-2}. MFC2 and MFC3 only reached 400 W cm^{-2} and 270 W cm^{-2}, respectively. However, when the glucose concentration increase to 100 mM (Fig. 4b), the power density of MFC1 significantly decreases, down to a value of 25 W cm^{-2} (less than a 10% of the power density obtained with 10 mM of glucose), but MFC2 do not experiences loss of power, contrarily MFC2 increase the power to 630 W cm^{-2}. MFC3 suffers a little loss of power to 230 W cm^{-2}.

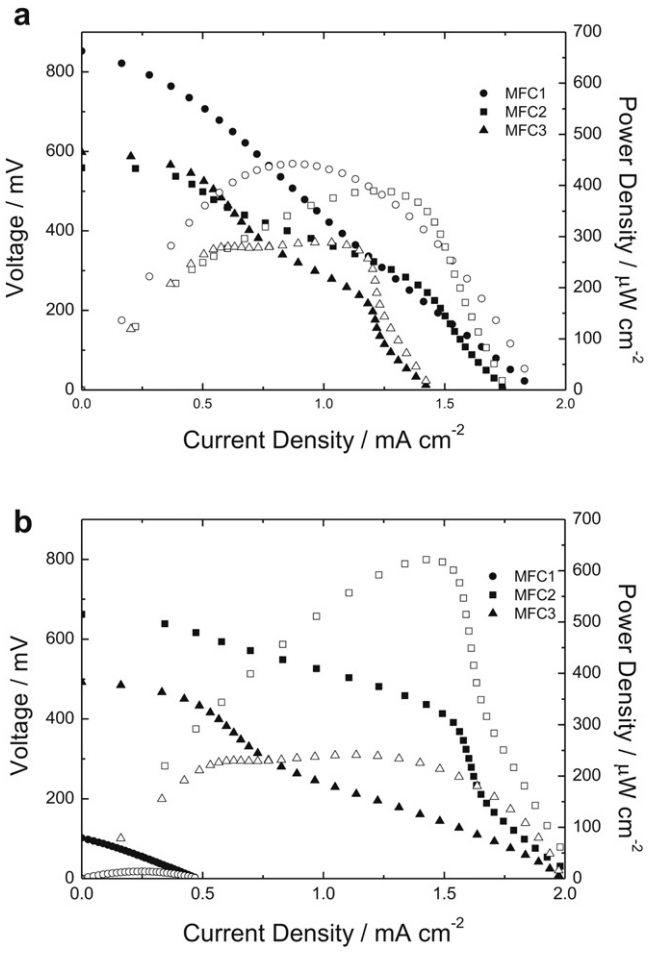

Fig. 4. Polarization curves of the three different cells (MFC1, MFC2 and MFC3) with separated laminar flows, a) glucose 10 mM and oxygen saturated in alkaline medium (0.3 KOH), b) glucose 100 mM and oxygen saturated in alkaline medium (0.3 KOH).

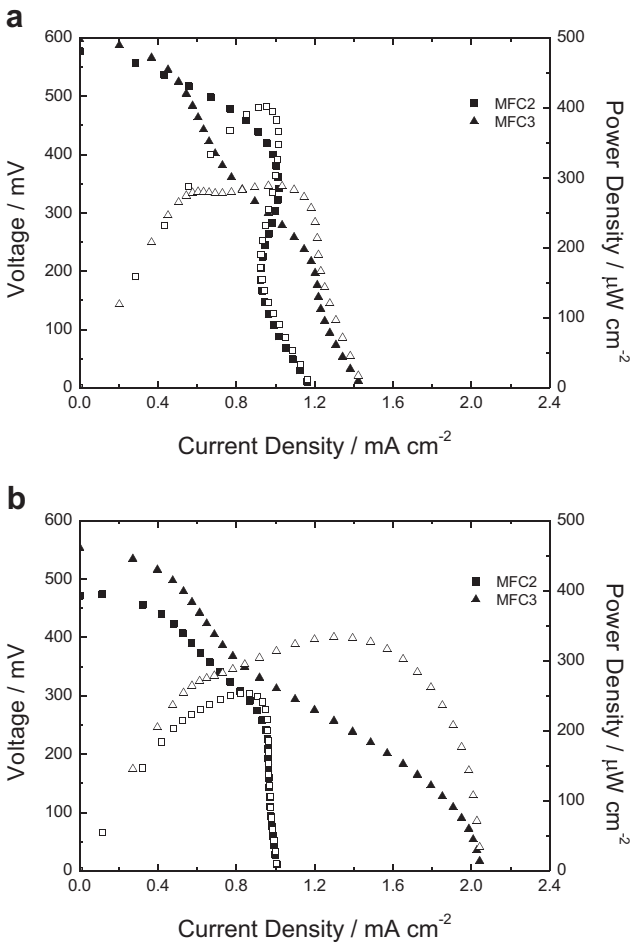

Fig. 5. Polarization curves of two different cells (MFC2 and MFC3) with a) a single combined flow of glucose 10 mM and oxygen saturated in alkaline medium (0.3 KOH), and b) a single combined flow of glucose 100 mM and oxygen saturated in alkaline medium (0.3 KOH).

In the case of a high glucose concentration 100 mM (G100), a strong crossover effect is promoted from the anode side to

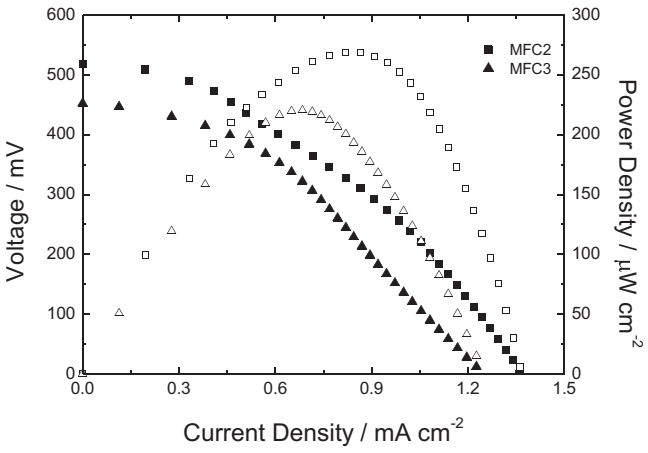

Fig. 6. Polarization curves of two different cells (MFC2 and MFC3) with a single combined flow of glucose 10 mM and oxygen saturated in alkaline SBF.

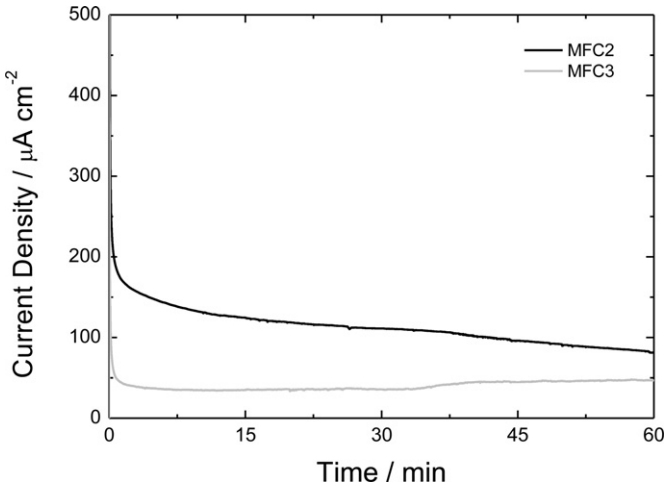

Fig. 7. Chronoamperometry of MFC2 and MFC3 in alkaline SBF.

cathode side, causing a loss of performance of the cell. But the PtAg is highly tolerant to glucose, reducing the consequences of cross-over effect. This result is consistent with previous work [31].

3.3. Microfluidic fuel cell performance with a single combined flow

Considering the high ORR selectivity, a unique fluid flow with a mixture of glucose (10 mM and 100 mM) and oxygen was employed. Polarization curves (Fig. 5a) obtained in the case of 10 mM glucose solution show that MFC2 has a better performance (400 μW cm^{-2}) than MFC3 (300 μW cm^{-2}). In the same conditions, MFC1 was unable to work. For the case of 100 mM of glucose (Fig. 5b), a better power density performance is observed for MFC3, increasing the power density to 340 μW cm^{-2}. On the other hand, MFC2 decreased its maximum power density to 250 μW cm^{-2}. It is important to mention that in these critical conditions (only one fluid flow and high glucose concentration 100 mM), the catalyst electrodes that incorporate silver show the best power density performance.

3.4. Microfluidic fuel cell performance with a single SBF flow

The preceding results, using a unique stream, open the possibility to use this fuel cell as a portable power source in a wide variety of devices, e.g. lab-on-chip applications for biological

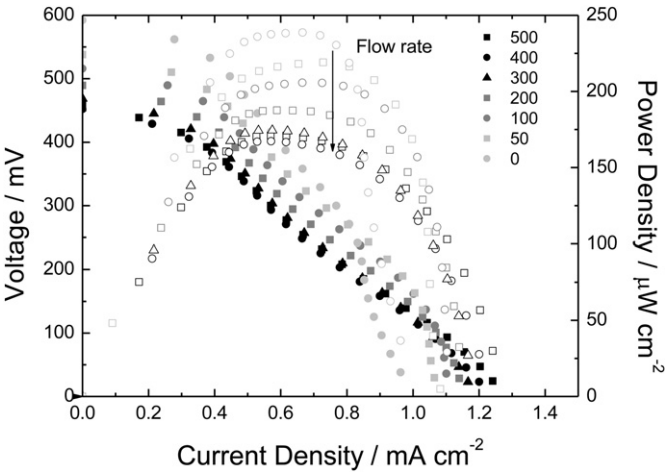

Fig. 8. Polarization curves for MFC3 in alkaline SBF at different flow rates.

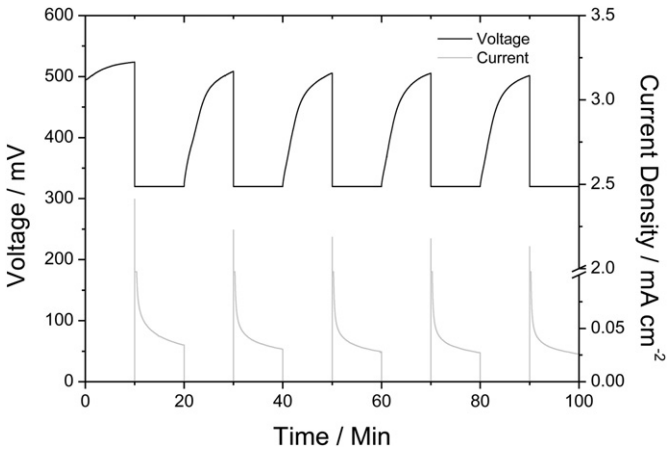

Fig. 9. Stability experiment for MFC3 in alkaline SBF with zero flow rate.

analysis. With this purpose, tests in simulated body fluid were performed. This medium has ionic species present in blood plasma, and is a good approach toward human fluid conditions.

All the cells were tested with SBF prepared with glucose and KOH. Maximum power densities of 270 μW cm^{-2} and 220 μW cm^{-2} were obtained from MFC2 and MFC3 respectively (Fig. 6). A loss of performance with respect to the single flow of glucose solution was observed. This is attributed to the solution ionic strength. Ionic strength has effects in the solution, influencing the activity coefficient and consequently the activity of species like OH^-. Hydroxide ion play an important role in the glucose oxidation as it has been demonstrated in literature [34]. The decrease in the activity of this species affects the reaction rate and decrease the power harvested by the cell.

On other hand, oxygen is less soluble in solution with high salt concentration. It decreases the voltage of the cell and the reaction rate on the cathodic side.

Fig. 7 shows the chronoamperometric tests carried out in SBF for MFC2 and MFC3. After 1 h, a reduction of the current in MFC2 was observed, but the performance in MFC3 was preserved. This result is attributed to poisoning on gold surface, according to the previous work; AuAg presents a higher resistance to poisoning [30].

3.5. Fuel cell performance at different flow rates

Due to its enhanced stability, MFC3 performance was evaluated at several flow rates. Fig. 8 shows the polarization curves of MFC3 for flow rates from 500 to 0 μL min^{-1}. Although the kinetics in the

Table 3
Electric parameters for stability test with zero flow fluid.

Parameter	Units	1	2	3	4	5
V_0	mV	523	509	506	505	502
j_0	mA cm^{-2}	2.41	2.23	2.19	2.18	2.13
j_f	μA cm^{-2}	34.4	30.5	28.0	27.1	25.9
P_0	μW cm^{-2}	771	714	701	698	682
P_f	μW cm^{-2}	10.9	9.76	8.96	8.67	8.29
VP_0	mW cm^{-3}	7.71	7.14	7.01	6.98	6.82
VP_f	μW cm^{-3}	109	97.6	89.6	86.7	82.9
Q	mC cm^{-2}	34.4	29.7	27.6	26.8	25.7
E	μWh	1.38	1.19	1.11	1.07	1.03

Table 4
Comparison of different glucose fuel cells.

Type	Anode/Cathode	Glucose Conc.	Conditions	Flow rate	Power density	Ref
BFC	GOD/BOD		Grape interior	Batch	2.6 μW cm^{-2}	[11]
BFC	CNT/ionic liquid/enzyme	10 mM	pH 5.86	Batch	2 μW cm^{-2}	[12]
BFC	GOD/BOD	10 mM	PBS pH 7	21.4 mL min^{-1}	30 μW cm^{-2}	[20]
MBFC	GOD/BOD	10 mM	C: pH 3, A: pH 7	0.1–1.0 mL min^{-1}	110 μW cm^{-2}	[19]
BFC	GDH-SWNHs-CFME/BOD-SWNHs-CFME	45 mM, 33 mM	Vegetable juice, aerated water	N/A	240 μW cm^{-2}	[21]
PEM	Au Ag UPD/Pt	10 mM	0.3 M NaOH	Batch	250 μW cm^{-2}	[15]
PEM	C/Pt–Bi–C	5 mM	PBS pH 7.4	Batch	3.3 μW cm^{-2} (after 10 days)	[16]
PEM	Pt Raney/Pt Raney	3 mM	PBS pH 7.4	Batch	4.5 μW cm^{-2}	[17]
PEM	Graphene/Pt	0.42%	PBS pH 7.4	N/A	5 μW cm^{-2}	[18]
PEM	Graphene/Pt	In vivo			10 μW cm^{-2}	[18]
Air-breathing PEM	Pt-CNT/Pt-CNT	0.5 M	pH 7.4	0.250 mL min^{-1}	0.768 μW cm^{-2}	[13]
MFC	Au–C/Pt	10 mM	0.3 M KOH	A: 0.042 mL min^{-1}, C: 0.110 mL min^{-1}	500 μW cm^{-2}	[9]
MFC	Au–C/PtAg–C	100 mM	0.3 KOH	A: 0.1 mL min^{-1}, C : 0.5 mL min^{-1}	620 μW cm^{-2}	This work
MFC	Au–C/PtAg–C	10 mM	0.3 KOH	Single flow 0.4 mL min^{-1}	410 μW cm^{-2}	This Work

BFC: Biofuel cell, MFC: Microfluidic fuel cell, MBFC: Microfluidic biofuel cell, C: Catholye, A: Anolyte.

cell are reduced because the material available to react is limited, the overall cell thermodynamics increases as the flow is decreased, how is observed with the cell voltage increasing from 450 mV to 600 mV. This behavior is caused by the better interaction between the reagents and the electrodes surfaces, related to the increase of residence time, as in a laminar flow reactor. The capability of this microfluidic fuel cell to work with zero flow fluid could make possible the elimination of external pumps. This gives many advantages such as smaller and less complex devices, no loss of energy in pumping, integration with biological systems and cost reductions.

3.6. Fuel cell stability with zero fluid flow

Finally, studies at flow zero were performed to evaluate the capability of the cell to work in prolonged periods without constant injection of fuel. The experiment was designed to prove the recovery capacity of cell and stability of the catalyst surface.

Fig. 9 shows the behavior of the cell voltage (black) and current density (gray) during the experiment. The results show a stability of five recharge and use cycles of 20 min each one. The graph of voltage shows stability in voltage terms, which is indicative of absence of surface poisoning. Current graphs show a peak of current in the first second, this is interesting for applications with demands of high power in short time (e.g. peacemakers), and a stability by 10 min with power density superior to 2 μW cm^{-2}.

Table 3 shows the electric parameters obtained from this experiment. These parameters are voltage before the chronoamperometry (V_0), current density instant (j_0) and constant (j_f), power density instant (P_0) and constant (P_f), volumetric power instant (VP_0) and constant (VP_f), charge density (Q) and energy density (E). Instant values correspond to the moment after the cell is switched from open circuit condition to the fixed voltage of 320 mV, while constant values are taken after the 10 min operating at this voltage. It could be observed that after each cycle, the microfluidic fuel cell was capable of harvest up to 96% of the electric energy delivered in the previous cycle.

Table 4 shows a comparison of different glucose fuel cells found in the literature. As it can be seen, the output power reported from these devices varies within a wide range of values. This is because of the different materials, designs and operation of the cells. The presented results from this work are the power density obtained from polarization curves with and without flow of reactants and also in the case of batch system, obtained from the stability test.

4. Conclusions

The operation of a glucose-based microfluidic fuel cell using a single flow of fuel and oxidant in alkaline media was demonstrated. The combination of high selectivity of PtAg/C in the ORR and AuAg/C in the GOR led to a remarkable performance, which opens a wide range of possibilities in future applications.

SBF test shows that fuel cells with PtAg/C in cathode were able to work in high ionic-concentrated solutions similar to extracellular fluid. Therefore these fuel cells prove a strong potential for incorporating in biocompatible devices.

It was also observed that the fuel cell power density increased with decreasing the fuel flow rate, reaching 50% more power at flow zero with respect to 500 μL min^{-1}. Furthermore, the fuel cell was able to work for several cycles at zero flow fluid. These experiments demonstrate the capability of the fuel cell to work without an external fuel pump. Hence, the fuel cell could operate driving the fuel by diffusion or capillary forces.

Acknowledgments

The authors thank the Mexican Council for Science and Technology for financial support through ANR-CONACYT 2011 (Grant 163114) and Fomix-Chihuahua 127461.

References

[1] D. Mark, S. Haeberle, G. Roth, F.V. Stetten, R. Zengerle, Chem. Soc. Rev. 39 (2010) 1153.
[2] S. Tominaka, H. Nishizeko, J. Mizuno, T. Osaka, Energy Environ. Sci. 2 (2009) 1074.
[3] E.R. Choban, L.J. Markoski, A. .Wieckowski, P.J.A. .Kenis, J. Power Sources 128 (2004) 54.
[4] E. Kjeang, N. Djiali, D. Sinton, J. Power Sources 186 (2009) 353.
[5] D. Morales-Acosta, H.G. Rodríguez, L.A. Godinez, L.G. Arriaga, J. Power Sources 195 (2010) 1862.
[6] D. Morales-Acosta, J. Ledesma-García, L.A. Godinez, H.G. Rodríguez, L. Álvarez-Contreras, L.G. Arriaga, J. Power Sources 195 (2010) 461.
[7] R.L. Arechederra, B.L. Treu, S.D. Minteer, J. Power Sources 173 (2007) 156.
[8] D. Morales-Acosta, L.G. Arriaga, L. Alvarez-Contreras, S. Fraire Luna, F.J. Rodríguez Varela, Electrochem. Commun. 11 (2009) 1414.

[9] M. Guerra-Balcázar, D. Morales-Acosta, F. Castañeda, J. Ledesma-García, L.G. Arriaga, Electrochem. Commun. 12 (2010) 864.
[10] S. Calabrese Barton, J. Gallaway, P. Atanassov, Chem. Rev. 104 (2004) 4867.
[11] J. Ryu, H.-S. Kim, H. Thomas Hahn, D. Lashmore, Biosens. Bioelectron. 25 (2010) 1603.
[12] A. Zebda, L. Renaud, M. Cretin, C. Innocent, F. Pichot, R. Ferrigno, S. Tingry, J. Power Sources 193 (2009) 602.
[13] Y. Liu, S. Dong, Biosens. Bioelectron. 23 (2007) 593.
[14] D. Scott, B.Y. Liaw, Energy Environ. Sci. 2 (2009) 965.
[15] C. Jin, I. Taniguchi, Mat. Lett. 61 (2007) 2365.
[16] S. Kerzenmacher, J. Ducrée, R. Zengerle, F. von Stetten, J. Power Sources 182 (2008) 66.
[17] S. Kerzenmacher, U. Kräling, T. Metz, R. Zengerle, F. Von Stetten, J. Power Sources 196 (2011) 1264.
[18] T. Sharma, Y. Hu, M. Stoller, M. Feldman, R.S. Ruoff, M. Ferrari, X. Zhang, Lab Chip. 11 (2011) 2460.
[19] N. Mano, F. Mao, A. Heller, J. Am. Chem. Soc. 124 (2002) 12962.
[20] A. Habrioux, G. Merle, K. Servat, K.B. Kokoh, C. Innocent, M. Cretin, S. Tingry, J. Electroanal. Chem. 622 (2008) 97.
[21] D. Wen, X. Xuab, S. Dong, Energy Environ. Sci. 4 (2011) 1358.
[22] M. Tominaga, T. Shimazoe, M. Nagashima, I. Taniguchi, Electrochem. Commun. 7 (2005) 189.
[23] L.D. Burke, P.F. Nugent, Gold Bull. 31 (1998) 39.
[24] M. Pasta, R. Ruffo, E. Falletta, C.M. Mari, C. Della Pina, Gold Bull. 43 (2010) 57.
[25] H. Quan, S.-U. Park, J. Park, Electrochim. Acta 55 (2010) 2232.
[26] J. Lin, C. He, Y. Zhao, S. Zhang, Sensor. Actuators B: Chem. 137 (2009) 768.
[27] M. Tominaga, T. Shimazoe, M. Nagashima, I. Taniguchi, J. Electroanal. Chem. 615 (2008) 51.
[28] S.B. Aoun, Z. Dursun, T. Koga, G.S. Bang, T. Sotomura, I. Taniguchi, J. Electroanal. Chem. 567 (2004) 175.
[29] Y. Feng, J. Ma, G. Zhang, D. Zhao, B. Xu, Chin. J. Catal. 30 (2009) 776.
[30] F.M. Cuevas-Muñiz, M. Guerra-Balcázar, F. Castaneda, J. Ledesma-García, L.G. Arriaga, J. Power Sources 196 (2011) 5853.
[31] M. Guerra-Balcázar, F.M. Cuevas-Muñiz, L. Álvarez-Contreras, L.G. Arriaga, J. Ledesma-García, J. Power Sources 197 (2012) 121.
[32] T. Kokubo, H. Takadama, Biomaterials 27 (2006) 2907.
[33] M. Brust, M. Walker, D. Bethell, D.J. Shiffrin, R. Whyman, J. Chem. Soc. Chem. Commun. 7 (1994) 801.
[34] M. Pasta, F. La Mantia, Y. Cuib, Electrochim. Acta 55 (2010) 5561.